In-situ growth and electronic structure modulation of urchin-like Ni–Fe oxyhydroxide on nickel foam as robust bifunctional catalysts for overall water splitting

*Zi ia Wan [a,1], Hongbo Yu [a,1], Qiuting He [a], Yan Hu [a], Pu uan Yan [a], Xue Shao [a], Ta irjan Ta lor Isimjan [c,**], Bing Zhang [b], Xiulin Yang [a,*]*

[a] *G ang i Ke Laborator of Le Carbon Energ Materials, School of Chemistr and Pharmace tical Sciences, G ang i Normal Uni ersit , G ilin, 541004, China*
[b] *National Instit te of Clean-and-Le -Carbon Energ , F t re Science Cit , Changping Dist., Beijing, 100085, China*
[c] *Sa di Arabia Basic Ind stries Corporation (SABIC) at King Abd llah Uni ersit of Science and Technolog (KAUST), Th e al, 23955-6900, Sa di Arabia*

HIGHLIGHTS

- Urchin-like FeOOH-NiOOH on Ni foam is constructed by a facile method.
- The catalyst exhibits excellent electrocatalytic performance for OER and HER.
- The two-electrode cell voltage is superior to RuO_2/NF(+)||Pt-C/NF(-) system.
- The synergy between Ni and Fe species dominate the excellent performance.

GRAPHICAL ABSTRACT

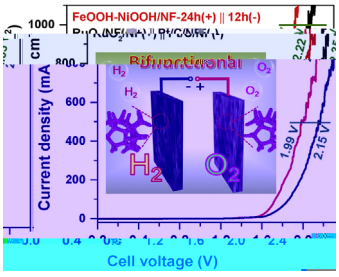

ARTICLE INFO

Article histor :
Received 25 April 2020
Received in revised form
17 June 2020
Accepted 19 June 2020
Available online 27 July 2020

Ke ords:
Iron-nickel oxyhydroxide

ABSTRACT

The rational design of non-precious-metal bifunctional catalysts of oxygen and hydrogen evolution reactions that generate a high current density and stability at low over potentials is of great significance in the field of water electrolysis. Herein, we report a facile and controllable method for the *in-sit* growth of urchin-like FeOOH–NiOOH catalyst on Ni foam (FeOOH–NiOOH/NF). X-ray photoelectron spectroscopy confirms that the proportion of Ni and Fe species with high valence state gradually increase with the extension of edthe4456.J/F31Tf14.704738.09e

Synergistic effect
Oxygen evolution
Overall water splitting
Cost estimate

at high current density (0.5–1.0 A cm^{-2}) as compared to the state-of the art RuO_2/NF(+)||Pt–C/NF(–) system, far better than most of the previously reported catalysts. The cost analyst revealed that using FeOOH–NiOOH/NF catalyst as both electrodes could potentially reduce the price of H_2 around 7% compared with traditional industrial electrolyzers. These excellent electrocatalytic properties can be attributed to the unique urchin-like structure and the synergy between Ni and Fe species, which can not only provide more active sites and accelerate electron transfer, but also promote electrolyte transport and gas emission.

Introduction

To produce H_2 through electrochemical water splitting as a most effective approach is heavily dependent on developing cost-effective catalysts that are easy to prepare, and rival the noble metal-based catalysts [1]. This process involves extending the oxygen evolution reaction (OER) and the hydrogen evolution reaction (HER) catalysts. Over the years, three main research directions have been merged in this field [2], namely active sites well-defined molecule catalyst tuned through functional ligands [3], traditional highly active but robust crystalline catalysts [4], and newly emerged versatile amorphous catalysts that surpasses both molecule and crystalline catalysts in many aspects [5]. The advantages of the amorphous catalysts are coming from their ability to endowing particular phase and oxidation changes that facilitate breaking and formation of new bonds thereof lower the activation energy. However, most of the highly active amorphous catalysts are based on either phosphate or sulfite materials that are not stable especially as OER catalysts [6]. Therefore, the metal oxide-based catalysts such as nickel-iron (hydr) oxide, cobalt iron bimetallic hydroxide, and nickel-cobalt compound are studied extensively. It is owing to their stability and the unique synergy between two different metals [7]. Specially, the Fe impurity in NiOOH generates detrimental effects on Ni-based alkaline electrodes by greatly lowering the OER over potential [8,9]. However, various attempts to understand the working mechanism of NiFe-based electro-catalysts have been conducted by different surface techniques [10,11] and density functional theory (DFT) calculations [12]. A widely accepted convincing, and congruous theory has yet to emerge due to the complexity of the problem [2].

However, those types of materials suffer from poor electronic conductivity that limits the practical application. As a result, many researchers put forward their effort on coupling catalysts with three-dimensional (3D) conductive supports to dramatically improve electrochemical performance, like as carbon cloth [13], nickel foam [14], graphene framework [15], and so on. Lina Liu et al. successfully synthetized efficient electrocatalyst to achieve overall water splitting through $FeNi_3N$ nanoparticles anchored on N-doped graphene [16]. Moreover, designing a bifunctional feature to this kind of catalyst not only reduces the catalyst cost but also increases the catalyst stability over higher voltage range [14,17]. Besides, the catalyst can easily be regenerated *in-sit ɨ* by bias-switching [18]. Despite the enormous progress in this field, there are only a few reports on high current density operation. For example, Feng Yan and co-workers fabricated a 3D NiFeOOH/CFC catalyst using *in-sit ɨ* electrochemical activations. The electrocatalyst has an excellent OER performance below 350 mA cm^{-2}. There was no report on the catalytic performance at high current density (>500 mA cm^{-2}) and overall water splitting applications [19]. Most importantly, none of the paper has discussed the industrial significance of the findings regarding its effect on the final price of H_2 generated through an industrial Electrolyzer. Based on the above considerations, we designed and prepared a low cost, high efficiency, and durable bifunctional catalyst that can be used at the high current density. Moreover, the cost of H_2 using this catalyst on an industrial scale is discussed.

In this work, the FeOOH–NiOOH/NF catalyst with highly conductive and exceptional activity is synthesized by a simple soaking method, which possesses bifunctional activity towards the OER and HER in alkaline solution. The FeOOH–NiOOH/NF can be directly utilized as an anode to deliver a high current density of 500 mA cm^{-2} for the OER at a much lower over potential of 280 mV as compare to RuO_2/NF. Meanwhile, it also requires low overpotential of 480 mV to reach the same current density using Pt–C/NF in 1.0 M KOH. Consequently, the FeOOH–NiOOH/NF two-electrode system steadily drives at the low cell voltages of 1.55 and 1.99 V to achieve the current densities of 10 and 500 mA cm^{-2} in an alkaline solution that are much smaller than these of RuO_2/NF||Pt–C/NF. To the best of our knowledge, the FeOOH–NiOOH/NF bifunctional system showed the lowest operation voltage reported so far. Interestingly, the system showed superior stability at high current density as compare to Pt–C/NF due to the integrated surface structure.

Experimental section

S nthesis of Ni(OH)$_2$/NF

Firstly, the nickel foam (NF) was cut into pieces with a size of 1 cm × 3 cm. The tailored NF was ultrasonically treated in turn by 0.5 M hydrochloric acid, deionized water, ethanol for 5 min respectively, and then dried at room temperature for use. Three pieces of NF were then immersed in 21 mL of a mixture containing 8 mL NaOH (5 M), 4 mL $(NH_4)S_2O_8$ (0.5 M), and 9 mL of deionized water at room temperature. After 30 min, the mixture was reacted with NF at 80 °C for 12 h. When cooled to

room temperature, the resulting NF is taken out and air-dried at 50 °C for 2 h. The $Ni(OH)_2$ arrays grown directly on NF was prepared by partial dissolution of NF. The resulting sample is denoted as $Ni(OH)_2$/NF.

S nthesis of Fe–Ni solution precursor

In a facile synthesis, 30 mL $FeCl_3$ (0.2 M) and 1 mL SDS (1.0 g L^{-1}) were uniformly dispersed by ultrasound for 30 min. Next, a piece of $Ni(OH)_2$/NF (1 cm × 3 cm) was immersed in the above mixture and transformed into a Teflon-lined stainless autoclave (50 mL) to react at 100 °C for about 12 h. After natural cooling to room temperature, the resulting mixture was allowed to rest for 12 h, then filtered to obtain the supernatant for backup, while the lower powder was dried at 60 °C for 3 h. It is worth mentioning that the obtained supernatant was used to prepare the target catalyst.

S nthesis of FeOOH–NiOOH/NF- h

The FeOOH–NiOOH *in-sit* grown on NF was fabricated by a facile immersion method. Specifically, a clean piece of NF (1 cm × 3 cm) is placed at an angle in the prepared supernatant at room temperature. The FeOOH–NiOOH/NF-xh catalyst was obtained by first soaking in the supernatant with different times (12, 24, 36, 48 h) and then drying at 50 °C for 3 h. As a result, the loading of catalysts is measured to be 0.53 mg cm^{-2} by a precision balance.

Electrochemical measurements

Electrochemical measurements were implemented by a VMP3B-2x2 electrochemical analyzer (CH Instruments, Inc, France) using a standard three-electrode system with a graphite plate as a counter electrode and saturated calomel electrode (SCE) as a reference electrode. Simultaneously, the catalysts loaded on NF (1 cm × 1 cm) were used as the working electrode. The loading of FeOOH–NiOOH catalysts on the NF is 0.53 mg cm^{-2}, and the 1.0 mg cm^{-2} of commercial RuO_2 or Pt/C was loaded onto NF for comparison. In a typical preparation procedure, the RuO_2 or Pt/C catalysts (5.0 mg) were dispersed in 450 μL ethanol, 450 μL distilled water, and 50 μL of 5% Nafion solution with sonication to acquire the homogeneous catalyst ink. Afterward, 190 μL of the ink was spread onto a piece of pretreated NF (1 cm × 1 cm) and dried at room temperature.

Electrochemical measurements of those catalysts were implemented in 1.0 M KOH solution. All the working electrodes were firstly excited to become a stable state by cyclic voltammetry (CV) at a scan rate of 10 mV s^{-1}, including OER, HER, and overall water splitting. The electrochemical data was recorded, and the polarization curves were acquired using linear sweep voltammetry (LSV) at a scan rate of 2 mV s^{-1}. Electrochemical impedance spectroscopy (EIS) measurements were carried out in the frequency range of 200 kHz–0.1 Hz. The chronopotentiometry was utilized for long-term stability tests. The electrochemical double-layer capacitances (C_{dl}) were carried out by CV measurements to determine the electrochemically active surface area (EASA) of the electrodes in a non-Faradaic region at scan rates of 100, 120, 140, 160, 180 and 200 mV s^{-1}. As a practical application, two pieces of FeOOH–NiOOH/NF catalysts (1 cm × 1 cm) were utilized as anode and cathode electrodes in a two-electrode system. The overall water splitting test was performed with a scan rate of 5 mV s^{-1} in 1.0 M KOH electrolyte at room temperature. All potentials were calibrated to RHE using the following equation: E(RHE) = E(SCE) + 1.040 V, which is consistent with the theoretical Nernst equation (Fig. S1). All electrochemical data are corrected against ohm potential drop by 100% *iR* compensation.

Result and discussion

S nthetic strateg anal sis

The fabricating process of FeOOH–NiOOH/NF is schematically illustrated in Scheme 1. First, the clean surface of NF is converted into a filamentary nickel hydroxide layer supported by NF in an alkaline solution by a thermal oxidation etching process and marked as $Ni(OH)_2$/NF. During the procedure, nickel is selectively oxidized into $Ni(OH)_2$, and then, the as-prepared $Ni(OH)_2$/NF as a source of nickel, which was further hydrothermally heated with $FeCl_3$ solution. During the thermal treatment, a Fe–Ni hydroxyoxide-rich solution was formed due to the continuous etching of Ni surface in the $FeCl_3$ solution (Fig. S2) [20]. When a piece of clean NF was immersed in the above suspension, urchin-like Ni–Fe oxyhydroxides were growth *in-sit* on the surface of NF, thereof different types of FeOOH–NiOOH/NF-xh (x = 12, 24, 36 or 48) materials were prepared over time (Fig. S3).

Cr stallinit and microstructure anal sis

The phase chemical composition and crystalline level of FeOOH–NiOOH/NF catalysts (Fig. S4) were analyzed by X-ray diffraction (XRD). Due to the sharp diffraction peaks of the metallic nickel of NF, the composition of the substance on the surface could not be detected. Hence, the scribed powder from the NF surface was used for characterization. As shown in Fig. 1a, the crystal structure of the catalyst shows a series of diffraction peaks of FeOOH (JCPDS: 34-1266) [21]. It means that there is abundant FeOOH species in the clarified solution separating from the nickel-iron mixture. In Fig. 1b, the existence of FeOOH is further confirmed by the Raman spectrum of FeOOH–NiOOH/NF-24 h, where two characteristic bands appeared at 243 cm^{-1} and 667 cm^{-1} [22–24]. In addition, Raman spectrum also shows a main band at 381 cm^{-1} that can be assigned to Fe_2O_3 impurity resulted from FeOOH decomposition upon heat treatment [25].

Meanwhile, the composite displays two peaks at 474 cm^{-1} and 554 cm^{-1} attributing to the vibration modes of Ni–O and Ni–OH respectively [26–28]. The both peaks were broadened with increasing Fe contents reflecting higher degrees of the disorder as well as the decreased crystallinity at high Fe/Ni ratios. Since the catalyst will start to dissociate, and the OER activity will decrease beyond a certain Fe/Ni ratio, the optimal performance can be achieved by changing the $FeCl_3$ etching time. The results show that the time is 24 h.

The surface morphology, nanostructure, and dispersion of the catalysts are examined by scanning electron microscopy

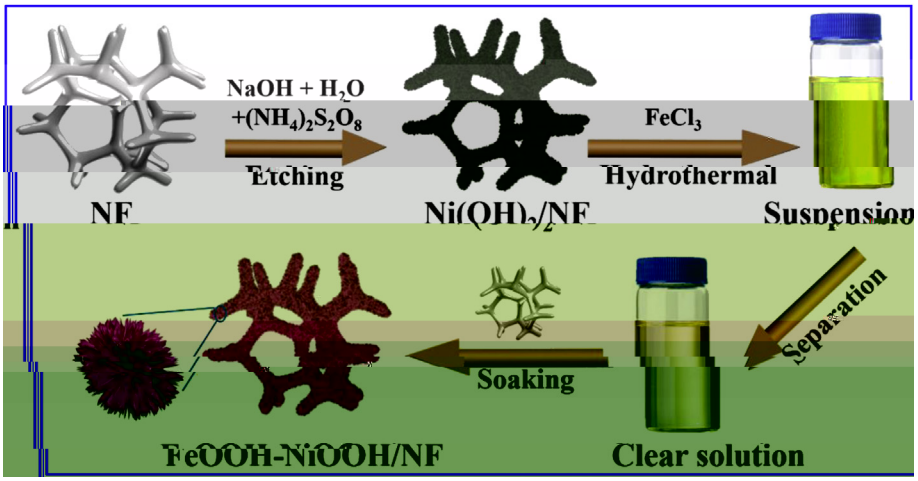

Scheme 1 – Schematic illustration of the synthesis process for FeOOH–NiOOH/NF.

(SEM) and transmission electron microscopy (TEM). Fig. S5 shows the microstructure of $Ni(OH)_2$/NF precursor, where $Ni(OH)_2$ species are anchored on the surface of NF with a vertical and interconnected sheet-like structure. After further processing, the SEM image appears to be a unique urchin-like structure of FeOOH–NiOOH/NF-24 h, which is constituted by highly oriented needle-like nanosheets (Fig. 1c). Besides, the SEM images of FeOOH–NiOOH/NF-xh materials obtained at different soaking times are shown in Fig. S6, which indicates crystal growth process starting from seeding (12 h), directional growth to urchin-like structures (24–36 h), and excessive aggregation (48 h). The TEM image illustrates that the thickness of the urchin-like structured FeOOH–NiOOH/NF-24 h is *ca.* 3.1 nm (Fig. 1d). Besides, the TEM demonstrates two types of clear lattice fringes, in which the lattice spacing of 0.236 nm points to the (301) plane of FeOOH, and the lattice spacing of 0.253 nm corresponds to the (101) plane of NiOOH (Fig. 1e). Moreover, the HAADF-STEM and elemental mappings of FeOOH–NiOOH/NF-24 h prove the uniform distribution of Ni, Fe, and O on the surface of the composite (Fig. 1f). These results indicate that the FeOOH–NiOOH/NF-24 h with urchin-like structure has a larger surface area, which can provide more active sites, contribute to electrolyte diffusion and gas release, and thereof significantly improve OER catalytic activity.

XPS anal sis

X-ray photoelectron spectroscopy (XPS) is further used to study the composition and chemical state of different materials. The survey spectrum (Fig. S7a) reveals the presence of C, O, Ni and Fe in the composites, where the high-resolution C 1s

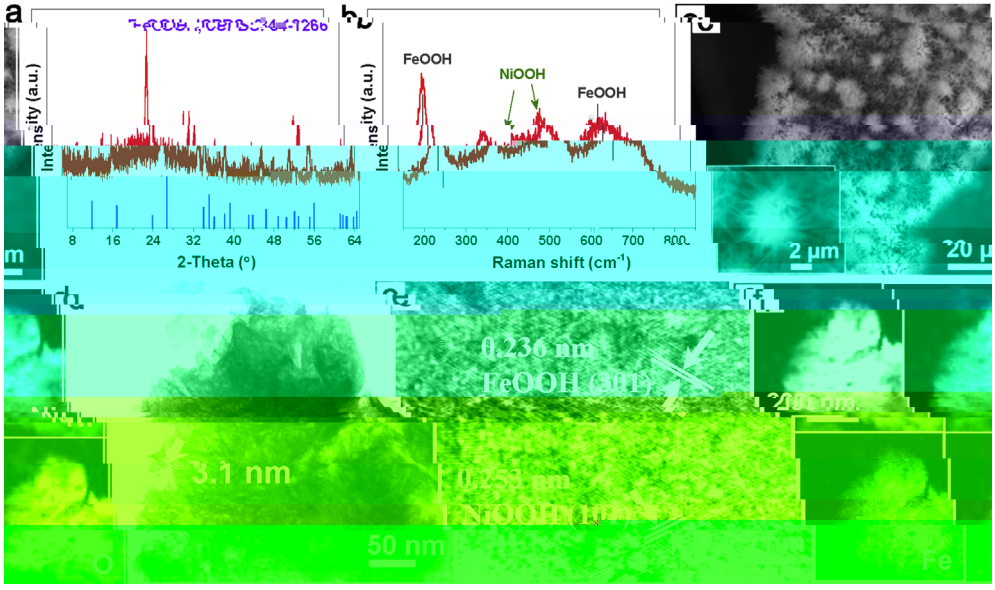

Fig. 1 – - (a) XRD pattern of collected powder. (b) Raman spectrum, (c) SEM image, (d) TEM image, (e) high-resolution TEM image, and (f) HAADF-STEM image and the corresponding elemental mappings of O, Ni and Fe from FeOOH–NiOOH/NF-24 h.

spectrum is deconvolved into C–C (284.8 eV), C–O (286.0 eV) and C=O (289.5 eV) as calibration standards (Fig. S7b) [29,30]. The M–O (529.8 eV), O–H (531.5 eV)) and O–O (533.0 eV) are acquired in the high-resolution O 1s spectrum (Fig. S7c), accordance with the literature reports [31,32]. A large O–O bond peak area indicates an oxyhydroxide rich environment [33] and the content of high-valence NiOOH species increased with the extension of soaking time. The peaks located at 852–870 eV correspond to Ni $2p_{3/2}$, which could be deconvolved into four peaks with various binding energies including NiO (853.8 eV), $Ni(OH)_2$ (855.6 eV), NiOOH (857.0 eV), and two concomitant satellites, respectively (Fig. 2a) [8,34]. Moreover, the high-resolution Fe 2p region of FeOOH–NiOOH/NF could be deconvolved into two significant peaks of Fe^{2+} (709.5 eV) and Fe^{3+} (711.0 eV) with the satellites at *ca.* 714.3 eV and 714.2 eV (Fig. 2b) [35,36].

Interestingly, the Fe^{3+}/Fe^{2+} gradually increased with the extension of the soaking time up to 48 h and the NiOOH film steadily collects the Fe impurities remaining in the solution. In general, formation of Fe–NiOOH shifts the OER onset potential to lower values due to the synergy between Fe and Ni which results an active O radical intermediate, while catalyzes the subsequent O–O coupling [37]. However, increasing Fe content, on the other hand, causes the lattice distortion thereof to decrease the catalyst stability. Therefore, an optimal point where the catalyst showed highest performance is expected upon the changing of the soaking time in the $FeCl_3$ solution. The bulk contents of Ni and Fe species in FeOOH–NiOOH/NF-xh, suspension and supernatant materials were determined by inductively coupled plasma spectrometer (ICP, Table S1) and Ni/Fe ratio was calculated accordingly.

OER catal tic performance

The OER activities of the catalysts were evaluated by linear sweep voltammetry (LSV) at a scan rate of 2 mV s^{-1} in 1.0 M KOH solution. All LSV polarization curves are processed by iR compensation (Fig. S8) and RHE correction due to the effect of ohmic resistance. For comparison, the RuO_2 (Aladdin Industrial Corporation, loads of 1.0 mg cm^{-2} on NF) catalyst is used as a control. Electrochemical impedance spectroscopy (EIS) is utilized to investigate the dynamics of interfacial electron transfer. As observed in Fig. S8, the FeOOH–NiOOH/NF-24 h has a much smaller semicircle and the charge-transfer impedance of approximately 0.84 Ω, comparing to other control materials. It means that the FeOOH–NiOOH/NF-24 h catalyst possesses a sizeable electrical conductivity as well as charge transfer kinetics at the electrode-electrolyte interface during the OER process [38].

Besides, the overpotential range of 0.1–0.2 V has a pair of strong Ni^{2+}/Ni^{3+} redox peaks from the polarization curves in Fig. 3a [39]. Notably, the FeOOH–NiOOH/NF-24 h catalyst exhibits excellent OER activity with an overpotential of 211 mV at the current density of 10 mA cm^{-2}, much lower than that of −12 h (232 mV), −36 h (222 mV), −48 h (239 mV) and commercial RuO_2 on NF (232 mV). Meanwhile, the FeOOH–NiOOH/NF-24 h catalyst also shows stable OER performance at high current density, requiring only 222, 280, and 329 mV overpotentials to achieve current densities of 100, 500 and 1000 mA cm^{-2} in the identical experimental setting. The results are much lower than most of the previously reported OER catalysts and RuO_2 control. To further validate the practical application, the etching solution was reused up to 9 times, and no apparent changes in OER performance of the FeOOH–NiOOH/NF-24 h at high current densities were observed (Fig. S9). As expected, it still outperforms most other control catalysts and previously reported catalysts at high

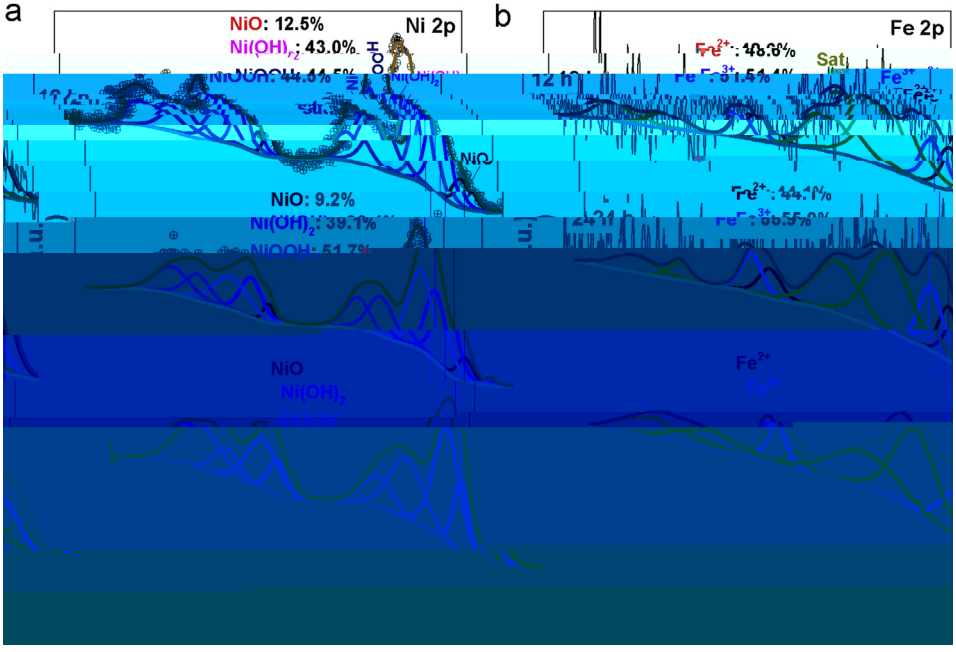

Fig. 2 – - High-resolution XPS spectra of (a) Ni 2p and (b) Fe 2p from FeOOH–NiOOH/NF-12 h, −24 h and −48 h, respectively.

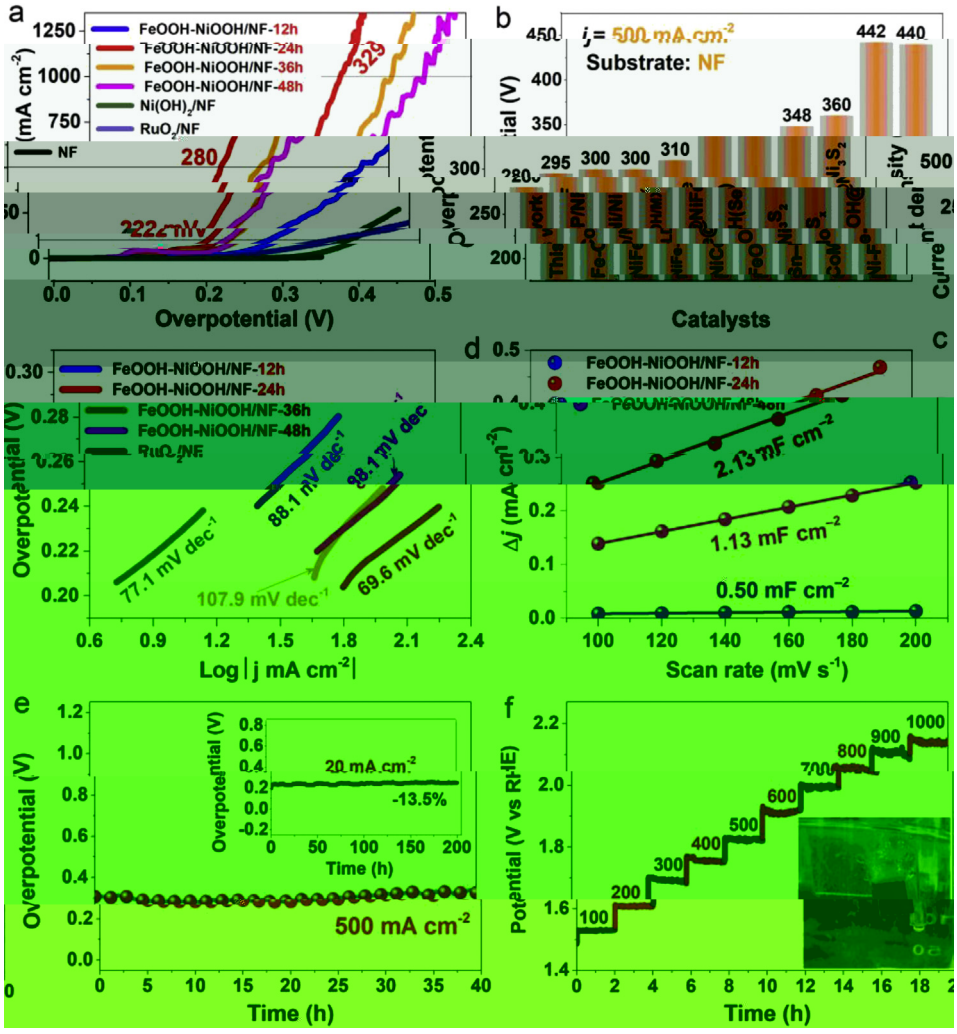

Fig. 3 – - OER catalytic performance of different catalysts in 1.0 M KOH. (a) LSV curves with a scan rate of 2 mV s^{-1}. (b) Comparison of OER activities among the published catalysts at a current density of 500 mA cm^{-2}. (c) Tafel slopes calculated from LSV curves. (d) The summarized double-layer capacitance (C_{dl}) of different catalysts. (e) Chronoamperometric test of FeOOH–NiOOH/NF-24 h catalyst at 500 mA cm^{-2} for 40 h (Inset: 20 mA cm^{-2} for 200 h). (f) Multi-step chronopotentiometric curves of FeOOH–NiOOH/NF-24 h from 100 to 1000 mA cm^{-2} with an increment of 100 mA cm^{-2} per 2 h (Inset: test photo).

current densities even after repeated use for several times indicating high durability (Fig. 3b and Table S2) [40–42].

Fig. 3c shows the corresponding Tafel slopes. The FeOOH–NiOOH/NF-24 h reveals a Tafel slope of 69.6 mV dec^{-1}, much smaller than those of –12 h (88.1 mV dec^{-1}), –36 h (107.9 mV dec^{-1}), –48 h (88.1 mV dec^{-1}), and even smaller than RuO_2 (77.1 mV dec^{-1}). Subsequently, the double-layer capacitance (C_{dl}) is also detected from the cyclic voltammetry (CV) curves at the non-Faradaic region with different scan rates (Fig. S10) [43]. As shown in Fig. 3d, the C_{dl} of the FeOOH–NiOOH/NF-24 h has the highest C_{dl} of 2.13 mF cm^{-2} than –12 h (0.50 mF cm^{-2}) and –48 h (1.13 mF cm^{-2}). Because electrochemical active surface area (EASA) is proportional to C_{dl}, the FeOOH–NiOOH/NF-24 h catalyst with the maximum C_{dl} value implies the highest EASA, consistent with the optimal OER catalytic activity as discussed above.

Furthermore, the long-term stabilities of the FeOOH–NiOOH/NF-24 h catalyst were tested at constant current densities of 20, and 500 mA cm^{-2} in a three-electrode system. The catalyst showed a high degree of stability under both cases (Fig. 3e). The kinetics of electrolyte diffusion, migration, and gas release during the electrochemical process was evaluated using a multi-step chronopotentiometry curve at various current densities ranging from 100 to 1000 mA cm^{-2} with an increment of 100 mA cm^{-2} per 2 h (Fig. 3f) [44]. These results indicate that the FeOOH–NiOOH/NF-24 h catalyst has excellent durability, which maybe attributes to its unique urchin-like structure, good electrical conductivity owing to the strong catalyst-support interaction. Moreover, the SEM images and XPS analysis after the long-term stability test of the FeOOH–NiOOH/NF-24 h (Figs. S11–13) reveal that the catalyst remains intact to the original morphology and high content of Ni^{3+} and Fe^{3+} species meaning maintained sufficient active sites. The above results further emphasize that the 3D urchin-like FeOOH–NiOOH/NF-24 h catalyst has excellent OER catalytic performance and stability at large current density.

In addition, the HER performances of FeOOH–NiOOH/NF-xh catalysts were also studied in 1.0 M KOH at room temperature. As shown in Fig. S14, the FeOOH–NiOOH/NF-12 h catalyst only requires an overpotential of 98 mV to reach −10 mA cm^{-2} (Fig. S14a), superior to all control catalysts and most previously reported catalysts in alkaline media (Table S3) [45–47]. The Tafel slope of FeOOH–NiOOH/NF-12 h catalyst is 127 mV dec^{-1}, which is much lower than that for −24 h of 204 mV dec^{-1} as well as −48 h of 239 mV dec^{-1} (Fig. S14b). It also indicated that the FeOOH–NiOOH/NF-12 h possesses fast reaction kinetics and the reaction rate is controlled by Volmer reaction at low current density [48]. Moreover, the optimal FeOOH–NiOOH/NF-12 h catalyst exhibits much lower charge-transfer impedance (R_{ct} = 0.94 Ω) than others (Fig. S14c), meaning a faster electronic transferability. Besides, the long-term durability tests show that the FeOOH–NiOOH/NF-12 h catalyst can maintain reliable high activity for 120 h at a current density of −10 mA cm^{-2} (Fig. S14d). The SEM image after the stability test is shown in Fig. S15. The results reveal that almost no changes in the FeOOH–NiOOH/NF-12 h catalyst morphology; therefore, the catalyst showed a stable performance even after 120 h of stability test. The FeOOH–NiOOH/NF-12 h exhibits excellent HER performance but moderate OER activity.

Overall water splitting

A two-electrode electrochemical system with FeOOH–NiOOH/NF-xh as the anode and cathode was constructed for overall water splitting to investigate the potential industrial application. As shown in Fig. 4a, the FeOOH–NiOOH/NF-24 h(+)||-12 h(−) electrolyzer delivers a current density of 10 mA cm^{-2} at a cell voltage of 1.55 V in 1.0 M KOH solution, lower than that of commercial RuO_2/NF(+)||Pt–C/NF(−) with cell voltage of 1.61 V. When the current densities reach 500 and 1000 mA cm^{-2}, the optimal catalysts only require cell voltages of 1.99 and 2.15 V respectively, which are lower than the commercial RuO_2/NF(+)||Pt/C/NF(−) catalysts with 0.16 and 0.13 V. Notably, the outstanding overall water splitting performance of our catalyst is further highlighted by comparing to other previously reported bifunctional electrocatalysts in alkaline media (Table S4) [49–52]. As expected, the optimal catalyst also demonstrated excellent two-electrode water splitting stability under high current conditions (Fig. 4b). More importantly, there was no obvious decay after continuous operation at 500 mA cm^{-2} for 100 h.

Cost estimate

The levelized cost of H_2 ($/kg) (LCOH) is calculated to estimate the cost reduction of the optimized electrocatalyst at the final price of the hydrogen produced by PEM electrolysis. The following assumptions were applied to achieve a reasonable estimate.

- The lifetime of the PEM Electrolyzer is 10 years.
- Return of investigating 20 years.
- The H_2 pressure is raging from 1 to 700 bar.
- Levelized cost of H_2 (LCOH) ($/kg) = Capital cost (Capex)/capacity × lifetime + Operating cost (Opex).
- Operating cost (Opex) = standard hydrogen consumption (kWh/Nm^3) × electricity price (electricity price).
- The state of art catalyst based electrolyzer cell voltage of 1.8 V at 600 mA cm^{-2} and 80 °C [53].
- The cost of electricity 7 cent/kwh [54].
- The voltage reduction using FeOOH–NiOOH/NF-24 h(+)//-12 h(−) at high current density (500–1000 mA cm^{-2}) is 0.15 V.

The cost estimation of the electrolytic system is based on market research prices and related literature [55,56]. The cost of the electrodes is around 8% of the total Electrolyzer's cost, and the industrial electrodes are stainless steel alloy consisting nickel, iron, and chromium therefore there is no significant cost-benefit by changing the electrodes to Fe–Ni based materials [57]. However, the main cost reduction comes from the lowering the cell voltage at same current density. Moreover, 80% of the LCOH is dominated by electricity price. The voltage reduction of 0.15 V using FeOOH–NiOOH/NF-24 h(+)||-12 h(−) at 30 bar can be translated into a power reduction of 3.7 kwh according to DOE H_2A Analysis meaning 0.32 $ saving for per kg of H_2 at 0.07$/kwh electricity price [58].

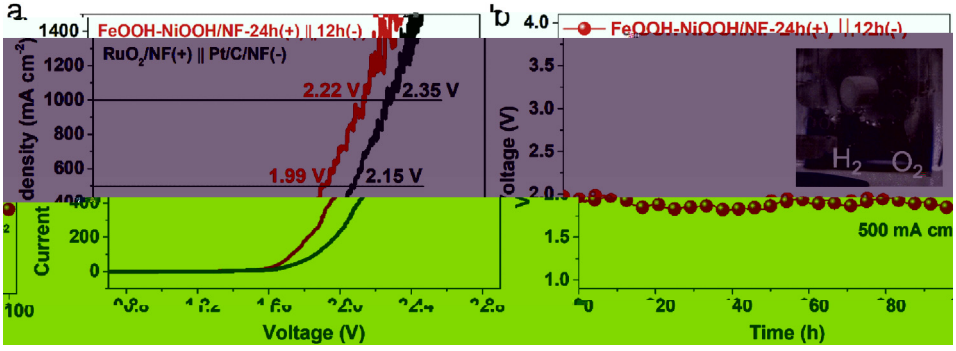

Fig. 4 – (a) Overall water splitting of different catalysts in two-electrode system. (b) Chronopotentiometric test of FeOOH–NiOOH/NF-24 h||-12 h catalysts at a fixed current density of 500 mA cm^{-2} for 100 h (Inset: test photo).

Conclusion

In summary, a 3D urchin-like FeOOH–NiOOH/NF catalyst is successfully fabricated by *the in-sit* / growth of FeOOH–NiOOH on NF in synthetic solution. The optimal FeOOH–NiOOH/NF showed outstanding bifunctional OER and HER properties at high current density (500–1000 mA cm^{-2}) as compared to the similar catalyst reported in the literature. As a binder-free electrode, the FeOOH–NiOOH/NF catalyst can decrease the voltage required by 0.15 V at the high current density and subsequently drop the price of H_2 by 0.32 $ for per kg of H_2 generated. This unique method has shown a promising industrial prospect.

Declaration of competing interest

The authors declare that they have no known competing financial interests or personal relationships that could have appeared to influence the work reported in this paper.

Acknowledgements

This work has been supported by the National Natural Science Foundation of China (no. 21965005), Natural Science Foundation of Guangxi Province (2018JJA120134, 2018GXNSFAA281220), Project of High-Level Talents of Guangxi (F-KA18015, 2018ZD004).

Appendix A. Supplementary data

Supplementary data related to this article can be found at https://doi.org/10.1016/j.ijhydene.2020.06.180.

REFERENCES

[1] Wang H, Dai H. Strongly coupled inorganic–nano-carbon hybrid materials for energy storage. Chem Soc Rev 2013;42:3088–113. https://doi.org/10.1039/C2CS35307E.

[2] Gong M, Dai H. A mini review of NiFe-based materials as highly active oxygen evolution reaction electrocatalysts. Nano Res 2015;8:23–39. https://doi.org/10.1007/s12274-014-0591-z.

[3] Yu W, Isimjan T, Gobbo SD, Anjum DH, Abdel-Azeim S, Cavallo L, Garcia-Esparza AT, Domen K, Xu W, Takanabe K. Tethering metal ions to photocatalyst particulate surfaces by bifunctional molecular linkers for efficient hydrogen evolution. ChemSusChem 2014;7:2575–83. https://doi.org/10.1002/cssc.201402297.

[4] Liu J, Zheng Y, Wang Z, Lu Z, Vasileff A, Qiao S-Z. Free-standing single-crystalline NiFe-hydroxide nanoflake arrays: a self-activated and robust electrocatalyst for oxygen evolution. Chem Commun 2018;54:463–6. https://doi.org/10.1039/C7CC08843D.

[5] Yan Q, Wei T, Wu J, Yang X, Zhu M, Cheng K, Ye K, Zhu K, Yan J, Cao D, Wang G, Pan Y. Self-supported FeNi-P nanosheets with thin amorphous layers for efficient electrocatalytic water splitting. ACS Sustainable Chem Eng 2018;6:9640–8. https://doi.org/10.1021/acssuschemeng.7b04743.

[6] Wang L, Duan X, Liu X, Gu J, Si R, Qiu Y, Qiu Y, Shi D, Chen F, Sun X, Lin J, Sun J. Atomically dispersed Mo supported on metallic Co_9S_8 nanoflakes as an advanced noble-metal-free bifunctional water splitting catalyst working in universal pH conditions. Adv Energy Mater 2020;10:1903137. https://doi.org/10.1002/aenm.201903137.

[7] Liang C, Zou P, Nairan A, Zhang Y, Liu J, Liu K, Hu S, Kang F, Fan HJ, Yang C. Exceptional performance of hierarchical Ni–Fe oxyhydroxide@NiFe alloy nanowire array electrocatalysts for large current density water splitting. Energy Environ Sci 2020;13:86–95. https://doi.org/10.1039/C9EE02388G.

[8] Wan Z, Yang D, Chen J, Tian J, Isimjan TT, Yang X. Oxygen-evolution catalysts based on iron-mediated nickel metal–organic frameworks. ACS Appl Nano Mater 2019;2:6334–42. https://doi.org/10.1021/acsanm.9b01330.

[9] Shin H, Xiao H, Goddard WA. In silico discovery of new dopants for Fe-doped Ni oxyhydroxide ($Ni_{1-x}Fe_xOOH$) catalysts for oxygen evolution reaction. J Am Chem Soc 2018;140:6745–8. https://doi.org/10.1021/jacs.8b02225.

[10] Landon J, Demeter E, İnoğlu N, Keturakis C, Wachs IE, Vasić R, Frenkel AI, Kitchin JR. Spectroscopic characterization of mixed Fe–Ni oxide electrocatalysts for the oxygen evolution reaction in alkaline electrolytes. ACS Catal 2012;2:1793–801. https://doi.org/10.1021/cs3002644.

[11] Diaz-Morales O, Ferrus-Suspedra D, Koper MTM. The importance of nickel oxyhydroxide deprotonation on its activity towards electrochemical water oxidation. Chem Sci 2016;7:2639–45. https://doi.org/10.1039/C5SC04486C.

[12] Xue Z, Zhang X, Qin J, Liu R. Revealing Ni-based layered double hydroxides as high-efficiency electrocatalysts for the oxygen evolution reaction: a DFT study. J Mater Chem 2019;7:23091–7. https://doi.org/10.1039/C9TA06686A.

[13] Wang B, Huang H, Huang M, Yan P, Isimjan TT, Yang X. Electron-transfer enhanced MoO_2-Ni heterostructures as a highly efficient pH-universal catalyst for hydrogen evolution. Sci China Chem 2020;63:841–9. https://doi.org/10.1007/s11426-019-9721-0.

[14] Yan P, Huang M, Wang B, Wan Z, Qian M, Yan H, Isimjan TT, Tian J, Yang X. Oxygen defect-rich double-layer hierarchical porous Co_3O_4 arrays as high-efficient oxygen evolution catalyst for overall water splitting. J Energy Chem 2020;47:299–306. https://doi.org/10.1016/j.jechem.2020.02.006.

[15] Peng X, Chen D, Yang X, Wang D, Li M, Tseng C-C, Panneerselvam R, Wang X, Hu W, Tian J, Zhao Y. Microwave-Assisted synthesis of highly dispersed PtCu nanoparticles on three-dimensional nitrogen-doped graphene networks with remarkably enhanced methanol electrooxidation. ACS Appl Mater Interfaces 2016;8:33673–80. https://doi.org/10.1021/acsami.6b11800.

[16] Liu L, Yan F, Li K, Zhu C, Xie Y, Zhang X, Chen Y. Ultrasmall $FeNi_3N$ particles with an exposed active (110) surface anchored on nitrogen-doped graphene for multifunctional electrocatalysts. J Mater Chem 2019;7:1083–91. https://doi.org/10.1039/C8TA10083G.

[17] Yang X, Li H, Lu A-Y, Min S, Idriss Z, Hedhili MN, Huang K-W, Idriss H, Li L-J. Highly acid-durable carbon coated Co_3O_4 nanoarrays as efficient oxygen evolution electrocatalysts. Nanomater Energy 2016;25:42–50. https://doi.org/10.1016/j.nanoen.2016.04.035.

[18] Kornienko N, Heidary N, Cibin G, Reisner E. Catalysis by design: development of a bifunctional water splitting catalyst through an operando measurement directed optimization cycle. Chem Sci 2018;9:5322–33. https://doi.org/10.1039/C8SC01415A.

[19] Yan F, Zhu C, Li C, Zhang S, Zhang X, Chen Y. Highly stable three-dimensional nickel–iron oxyhydroxide catalysts for oxygen evolution reaction at high current densities. Electrochim Acta 2017;245:770–9. https://doi.org/10.1016/j.electacta.2017.05.200.
[20] Zhu C, Yin Z, Lai W, Sun Y, Liu L, Zhang X, Chen Y, Chou S-L. Fe-Ni-Mo nitride porous nanotubes for full water splitting and Zn-air batteries. Adv Energy Mater 2018;8:1802327. https://doi.org/10.1002/aenm.201802327.
[21] Meng H, Ren Z, Du S, Wu J, Yang X, Xue Y, Fu H. Engineering a stereo-film of $FeNi_3$ nanosheet-covered FeOOH arrays for efficient oxygen evolution. Nanoscale 2018;10:10971–8. https://doi.org/10.1039/C8NR02770F.
[22] Kim B-J, Cheng X, Abbott DF, Fabbri E, Bozza F, Graule T, Castelli IE, Wiles L, Danilovic N, Ayers KE, Marzari N, Schmidt TJ. Highly active nanoperovskite catalysts for oxygen evolution reaction: insights into activity and stability of $Ba_{0.5}Sr_{0.5}Co_{0.8}Fe_{0.2}O_{2+\delta}$ and $PrBaCo_2O_{5+\delta}$. Adv Funct Mater 2018;28:1804355. https://doi.org/10.1002/adfm.201804355.
[23] Suryawanshi MP, Ghorpade UV, Shin SW, Suryawanshi UP, Jo E, Kim JH. Hierarchically coupled Ni:FeOOH nanosheets on 3D N-doped graphite foam as self-supported electrocatalysts for efficient and durable water oxidation. ACS Catal 2019;9:5025–34. https://doi.org/10.1021/acscatal.9b00492.
[24] Molchan IS, Thompson GE, Lindsay R, Skeldon P, Likodimos V, Romanos GE, Falaras P, Adamova G, Iliev B, Schubert TJS. Corrosion behaviour of mild steel in 1-alkyl-3-methylimidazolium tricyanomethanide ionic liquids for CO_2 capture applications. RSC Adv 2014;4:5300–11. https://doi.org/10.1039/C3RA45872E.
[25] Rehman S, Yang W, Liu F, Hong Y, Wang T, Hou Y. Facile synthesis of anisotropic single crystalline α-Fe_2O_3 nanoplates and their facet-dependent catalytic performance. Inorg Chem Front 2015;2:576–83. https://doi.org/10.1039/C5QI00042D.
[26] Jin Y, Huang S, Yue X, Du H, Shen PK. Mo- and Fe-modified $Ni(OH)_2$/NiOOH nanosheets as highly active and stable electrocatalysts for oxygen evolution reaction. ACS Catal 2018;8:2359–63. https://doi.org/10.1021/acscatal.7b04226.
[27] Tang C, Cheng N, Pu Z, Xing W, Sun X. NiSe nanowire film supported on nickel foam: an efficient and stable 3D bifunctional electrode for full water splitting. Angew Chem Int Ed 2015;54:9351–5. https://doi.org/10.1002/anie.201503407.
[28] Zhou F, Tien HN, Xu WL, Chen J-T, Liu Q, Hicks E, Fathizadeh M, Li S, Yu M. Ultrathin graphene oxide-based hollow fiber membranes with brush-like CO_2-philic agent for highly efficient CO_2 capture. Nat Commun 2017;8:2107. https://doi.org/10.1038/s41467-017-02318-1.
[29] Qian M, Xu M, Zhou S, Tian J, Taylor Isimjan T, Shi Z, Yang X. Template synthesis of two-dimensional ternary nickel-cobalt-nitrogen co-doped porous carbon film: promoting the conductivity and more active sites for oxygen reduction. J Colloid Interface Sci 2020;564:276–85. https://doi.org/10.1016/j.jcis.2019.12.089.
[30] Guo J, Wang B, Yang D, Wan Z, Yan P, Tian J, Isimjan TT, Yang X. Rugae-like Ni_2P-CoP nanoarrays as a bi-functional catalyst for hydrogen generation: $NaBH_4$ hydrolysis and water reduction. Appl Catal B Environ 2020;265:118584. https://doi.org/10.1016/j.apcatb.2019.118584.
[31] Zhang D, Kong X, Jiang M, Lei D, Lei X. NiOOH-decorated α-FeOOH nanosheet array on stainless steel for applications in oxygen evolution reactions and supercapacitors. ACS Sustainable Chem Eng 2019;7:4420–8. https://doi.org/10.1021/acssuschemeng.8b06386.
[32] Deng J, Zhang Q, Feng K, Lan H, Zhong J, Chaker M, Ma D. Efficient photoelectrochemical water oxidation on hematite with dual cocatalysts of fluorine-doped FeOOH and FeNiOOH. ChemSusChem 2018;11:3783–9. https://doi.org/10.1002/cssc.201801751.
[33] Dong C, Kou T, Gao H, Peng Z, Zhang Z. Eutectic-derived mesoporous Ni-Fe-O nanowire network catalyzing oxygen evolution and overall water splitting. Adv Energy Mater 2017;8:1701347. https://doi.org/10.1002/aenm.201701347.
[34] Zhou W, Lu X-F, Chen J-J, Zhou T, Liao P-Q, Wu M, Li G-R. Hierarchical porous prism arrays composed of hybrid Ni–NiO–Carbon as highly efficient electrocatalysts for overall water splitting. ACS Appl Mater Interfaces 2018;10:38906–14. https://doi.org/10.1021/acsami.8b13542.
[35] Yan L, Junheng H, Xiang H, Linlin B, Pingwei C, Jingchun J, Guoliang C, Shiqiang W, Liming D, Zhenhai W. Fe vacancies induced surface FeO_6 in nanoarchitectures of N-doped graphene protected β-FeOOH: effective active sites for pH-universal electrocatalytic oxygen reduction. Adv Funct Mater 2018;28:1803330. https://doi.org/10.1002/adfm.201803330.
[36] Zhang G, Qin Q, Luo W, Liu Y, Jin C, Hao J, Zhang J, Zheng W. A combination–decomposition method to synthesize two-dimensional metal sulfide–amine hybrid nanosheets: a highly efficient Fe-based water oxidation electrocatalyst. Chem Commun 2018;54:4617–20. https://doi.org/10.1039/C8CC00895G.
[37] Xiao H, Shin H, Goddard WA. Synergy between Fe and Ni in the optimal performance of (Ni,Fe)OOH catalysts for the oxygen evolution reaction. Proc Natl Acad Sci Unit States Am 2018;115:5872–7. https://doi.org/10.1073/pnas.1722034115.
[38] Nsanzimana JMV, Gong L, Dangol R, Reddu V, Jose V, Xia BY, Yan Q, Lee J-M, Wang X. Tailoring of metal boride morphology via anion for efficient water oxidation. Adv Energy Mater 2019;9:1901503. https://doi.org/10.1002/aenm.201901503.
[39] Xiang R, Tong C, Wang Y, Peng L, Nie Y, Li L, Huang X, Wei Z. Hierarchical coral-like $FeNi(OH)_X$/Ni via mild corrosion of nickel as an integrated electrode for efficient overall water splitting. Chin J Catal 2018;39:1736–45. https://doi.org/10.1016/S1872-2067(18)63150-X.
[40] Shan X, Liu J, Mu H, Xiao Y, Mei B, Liu W, Lin G, Jiang Z, Wen L, Jiang L. An engineered superhydrophilic/superaerophobic electrocatalyst composed of the supported CoMoSx chalcogel for overall water splitting. Angew Chem Int Ed 2020;58:2–9. https://doi.org/10.1002/anie.201911617.
[41] Wang PC, Wan L, Lin YQ, Wang BG. NiFe hydroxide supported on hierarchically porous nickel mesh as a high-performance bifunctional electrocatalyst for water splitting at large current density. ChemSusChem 2019;12:4038–45. https://doi.org/10.1002/cssc.201901439.
[42] Niu S, Jiang W-J, Wei Z, Tang T, Ma J, Hu J-S, Wan L-J. Se-doping activates FeOOH for cost-effective and efficient electrochemical water oxidation. J Am Chem Soc 2019;141:7005–13. https://doi.org/10.1021/jacs.9b01214.
[43] Wang B, Huang H, Sun T, Yan P, Isimjan TT, Tian J, Yang X. Dissolution reconstruction of electron-transfer enhanced hierarchical NiS_x-MoO_2 nanosponges as a promising industrialized hydrogen evolution catalyst beyond Pt/C. J Colloid Interface Sci 2020;567:339–46. https://doi.org/10.1016/j.jcis.2020.02.027.
[44] Yu M, Wang Z, Liu J, Sun F, Yang P, Qiu J. A hierarchically porous and hydrophilic 3D nickel–iron/MXene electrode for accelerating oxygen and hydrogen evolution at high current densities. Nanomater Energy 2019;63:103880. https://doi.org/10.1016/j.nanoen.2019.103880.
[45] Xiong P, Zhang X, Wan H, Wang S, Zhao Y, Zhang J, Zhou D, Gao W, Ma R, Sasaki T, Wang G. Interface modulation of two-dimensional superlattices for efficient overall water splitting. Nano Lett 2019;19:4518–26. https://doi.org/10.1021/acs.nanolett.9b01329.

[46] Huang K, Dong R, Wang C, Li W, Sun H, Geng B. Fe–Ni layered double hydroxide arrays with homogeneous heterostructure as efficient electrocatalysts for overall water splitting. ACS Sustainable Chem Eng 2019;7:15073–9. https://doi.org/10.1021/acssuschemeng.9b03731.

[47] Wang H, Xiao X, Liu S, Chiang C-L, Kuai X, Peng C-K, Lin Y-C, Meng X, Zhao J, Choi J, Lin Y-G, Lee J-M, Gao L. Structural and electronic optimization of MoS_2 edges for hydrogen evolution. J Am Chem Soc 2019;141:18578–84. https://doi.org/10.1021/jacs.9b09932.

[48] Mahmood N, Yao Y, Zhang JW, Pan L, Zhang X, Zou JJ. Electrocatalysts for hydrogen evolution in alkaline electrolytes: mechanisms, challenges, and prospective solutions. Adv Sci 2018;5:1700464. https://doi.org/10.1002/advs.201700464.

[49] Lai W, Zhang L, Hua W, Indris S, Yan Z, Hu Z, Zhang B, Liu Y, Wang L, Liu M, Wang Y, Wang J, Hu Z, Liu H, Chou S, Dou S. General π-electron-assisted strategy for constructing transition metal single-atom electrocatalysts with bi-functional active sites toward highly efficient water splitting. Angew Chem Int Ed 2019;58:11868–73. https://doi.org/10.1002/anie.201904614.

[50] Che Q, Li Q, Tan Y, Chen X, Xu X, Chen Y. One-step controllable synthesis of amorphous (Ni-Fe)S_x/NiFe$(OH)_y$ hollow microtube/sphere films as superior bifunctional electrocatalysts for quasi-industrial water splitting at large-current-density. Appl Catal B Environ 2019;246:337–48. https://doi.org/10.1016/j.apcatb.2019.01.082.

[51] Hao W, Wu R, Huang H, Ou X, Wang L, Sun D, Ma X, Guo Y. Fabrication of practical catalytic electrodes using insulating and eco-friendly substrates for overall water splitting. Energy Environ Sci 2020;13:102–10. https://doi.org/10.1039/C9EE00839J.

[52] Zhang Q, Bedford NM, Pan J, Lu X, Amal R. A fully reversible water electrolyzer cell made up from FeCoNi (Oxy)hydroxide atomic layers. Adv Energy Mater 2019;9:1901312. https://doi.org/10.1002/aenm.201901312.

[53] Xiang C, Papadantonakis KM, Lewis NS. Principles and implementations of electrolysis systems for water splitting. Mater Horiz 2016;3:169–73. https://doi.org/10.1039/C6MH00016A.

[54] Wang T. U.S. industrial consumer price of retail electricity 1970-2019. https://www.statista.com/statistics/190680/us-industrial-consumer-price-estimates-for-retail-electricity-since-1970/.

[55] Parks G, Boyd R, Cornish J, Remick R. Hydrogen station compression, storage, and dispensing technical status and costs: systems integration. Golden, CO (United States): National Renewable Energy Lab. (NREL); 2014. Medium: ED; Size: 74 pp, https://www.osti.gov/biblio/1130621/.

[56] Eichman J, Townsend A, Melaina M. Economic assessment of hydrogen technologies participating in California electricity markets. Golden, CO (United States): National Renewable Energy Lab. (NREL); 2016. Medium: ED; Size: 31 pp. https://www.osti.gov/biblio/1239543.

[57] Holladay JD, Hu J, King DL, Wang Y. An overview of hydrogen production technologies. Catal Today 2009;139:244–60. https://doi.org/10.1016/j.cattod.2008.08.039.

[58] Yin Z, Sun Y, Zhu C, Li C, Zhang X, Chen Y-J. Bimetallic Ni-Mo nitride nanotubes as highly active and stable bifunctional electrocatalysts for full water splitting. J Mater Chem 2017;5:13648–58. https://doi.org/10.1039/C7TA02876H.